Temporal and Spatial Autocorrelations from Expendable Digital Dropsondes (XDDs) in Tropical Cyclones

T. CONNOR NELSON[a] AND LEE HARRISON

Atmospheric Sciences Research Center, University at Albany, State University of New York, Albany, New York

KRISTEN L. CORBOSIERO

Department of Atmospheric and Environmental Sciences, University at Albany, State University of New York, Albany, New York

(Manuscript received 24 February 2019, in final form 30 December 2019)

ABSTRACT

The newly developed Expendable Digital Dropsondes (XDDs) allow for high spatial and temporal resolution observations of the kinematic and thermodynamic structures in tropical cyclones (TCs). It is important to evaluate both the temporal and spatial autocorrelations within the recorded data to address concerns about spatial interpolation, statistical significance of individual data points, and launch-rate spatial requirements for future dropsonde studies in TCs. Data from 437 XDDs launched into Hurricanes Marty (27–28 September), Joaquin (2–5 October), and Patricia (20–23 October) during the 2015 Tropical Cyclone Intensity (TCI) experiment are used to compute temporal and spatial autocorrelations for vertical velocity, temperature, horizontal wind speed, and equivalent potential temperature. All of the examined variables had temporal autocorrelation scales between approximately 10 and 40 s, with most between 20 and 30 s. Most of the spatial autocorrelation scales were estimated to be 3–10 km. The temporal autocorrelation scales for vertical velocity, horizontal wind speed, and equivalent potential temperature were correlated with updraft depth. Vertical velocity usually had the smallest mean, and median, temporal and estimated spatial autocorrelation scales of approximately 20 s and 3–6 km, respectively. The estimated horizontal scales are below the median sounding spacing and suggest that an increase in the launch rate of the XDDs by a factor of 3–4 from the TCI sampling rate is needed to adequately depict TC kinematics and structure in transects of soundings. The results also indicate that current temporal sampling rates are adequate to depict TC kinematics and structure in a single sounding.

1. Introduction

The Office of Naval Research conducted the Tropical Cyclone Intensity (TCI) experiment in 2015 (Doyle et al. 2017). Three of the tropical cyclones (TCs) that were sampled during TCI are Marty (27–28 September), Joaquin (2–5 October), and Patricia (20–23 October). A total of 725 global positioning system (GPS) dropwindsondes (hereinafter referred to as "dropsondes") were launched into these three TCs. The dropsondes used were the Expendable Digital Dropsondes (XDDs) manufactured by Yankee Environmental Systems, Inc., deployed using the High-Definition Sounding System (HDSS) on board a National Aeronautics and Space Administration WB-57 aircraft. The HDSS can launch one dropsonde every 10 s (Black et al. 2017), but during the 2015 TCI experiment, the quickest launch rate was 20 s at 4-km horizontal spacing (Doyle et al. 2017). The XDDs recorded atmospheric pressure p, temperature T, and relative humidity RH at 2 Hz and dropsonde horizontal motion components and GPS fall speed at a rate of 4 Hz (Black et al. 2017). The zonal (u) and meridional (v) wind components were computed directly from the dropsonde horizontal motion components. Vertical velocity w can be computed from the GPS fall speed or a calculated differential pressure fall speed (Nelson et al. 2019).

The HDSS and its capability to launch a large number of XDDs in quick succession provided unprecedented, high-temporal-and-spatial-resolution dropsonde observations

Supplemental information related to this paper is available at the Journals Online website: https://doi.org/10.1175/JTECH-D-19-0032.s1.

[a] Current affiliation: Department of Atmospheric and Oceanic Sciences, University of Colorado Boulder, Boulder, Colorado.

Corresponding author: T. Connor Nelson, ccnelson@albany.edu

DOI: 10.1175/JTECH-D-19-0032.1

during TCI. Because of the high sampling rate of the XDDs, it is possible that successive data points in a sounding, or data points from adjacent soundings, were appreciably correlated (i.e., correlation values greater than 0.5; Brooks and Carruthers 1978), and likely represented the same atmospheric phenomena, such as an updraft or small-scale vorticity maximum. To the best of the authors' knowledge, no study has considered the temporal and spatial autocorrelations (Brett and Tuller 1991; Griffith 2003; Khalili et al. 2007) of dropsondes in TCs. Only one study, Black et al. (1996), has directly examined the spatial autocorrelations of radar data in TCs. Analysis of the temporal and spatial autocorrelations of the TCI soundings are important to 1) aid targeted dropsonde or dropsonde deniability studies (studies examining the impact of removing observational data to be assimilated into a model; e.g., Mu et al. 2009; Torn and Hakim 2009; Wu et al. 2009; Romine et al. 2016), 2) evaluate what coherent features are resolvable by the dropsondes, 3) perform accurate spatial interpolation of any recorded variable, and 4) provide guidance as to what horizontal spacing is required to resolve various aspects of TC structure within transects of soundings.

The autocorrelations of data from nearby soundings is important in TC track and intensity modeling studies, and is especially important for studies examining the impact of targeted dropsonde observations and dropsonde data deniability (Langland 2005; Mu et al. 2009; Torn and Hakim 2009; Wu et al. 2009; Irvine et al. 2011; Romine et al. 2016), the crux of which is to examine the influence of data from a dropsonde, or set of dropsondes, at a specific location to the model forecast. The current approach for targeted dropsonde studies is to launch 10–50 dropsondes, with high-quality observations, intermittently in a predetermined sensitive area and assimilate the data into the model to improve the forecast (e.g., Langland 2005; Romine et al. 2016). Sensitive areas are determined by examining the effect of perturbing the initial conditions in a model, or by examining total energy singular vectors or ensemble transforms (Langland 2005; Mu et al. 2009). The goal is to assimilate numerous observations with small individual influence rather than one or two highly influential observations (Langland 2005). Increasing the number of observations and the observational horizontal resolution improves model forecasts if the observational errors are uncorrelated (Liu and Rabier 2003). If the observational errors are correlated, then increasing the number of observations beyond a set threshold does not improve the forecast (Liu and Rabier 2003).

Other studies have found that the resolution of the model and the correlation scale of the background model errors are important to determine the observational spacing required for targeted studies (e.g., Leutbecher et al. 2002; Liu and Rabier 2002, 2003; Aberson 2008; Torn and Hakim 2009). Leutbecher et al. (2002) state that soundings assimilated into models should be spaced 1–2 times the horizontal correlation length scale of the background model error. The length scale of the background model error varies from approximately 90 to 350 km depending on the model, resolution of the model, and the variable considered (Andersson et al. 1993; Irvine et al. 2011; Rizvi et al. 2012; Wang et al. 2014). Liu and Rabier (2002) found that the optimal observation spacing is approximately equal to the product of the analysis mesh size and the ratio of the number of grid points to the number of observations.

Knowledge of the temporal and spatial autocorrelations of dropsondes is also required in order to accurately depict TC structure from transects of dropsondes or aircraft. Some studies indicate that, to resolve features on the scale of the radius of maximum wind (RMW), grid spacing of approximately 14 km or less is required (Gentry and Lackmann 2010). The results of Gentry and Lackmann (2010), however, show that increased model resolution down to 2-km grid spacing or less is required to understand TC eyewall kinematics and physics. These results suggest that observations should also be taken at high resolution. The likelihood of highly correlated data points increases, however, with the increase in horizontal or vertical resolution and should approach unity (Brett and Tuller 1991; Khalili et al. 2007). Conversely, if dropsondes are launched too far apart, the thermodynamic and kinematic structure of a TC will not be well resolved or represented. Similarly, if data in a single sounding are recorded at low frequency, the thermodynamic and kinematic structure of a TC will not be well resolved or represented.

Examination of the temporal and spatial autocorrelations in the XDDs is critical to accurately perform any objective spatial interpolation. One interpolation scheme, called kriging, is a geostatistical interpolation method that uses covariance information to interpolate data fields (e.g., Biau et al. 1999). If adjacent data points in space or time are appreciably correlated, well modeled, or vary slowly in time and space, interpolation can easily be conducted between the data points (Gorman 2009). If adjacent data points are not appreciably correlated, however, then interpolation cannot be as easily conducted and could create unrealistic and uncharacteristic TCs by smoothing or smearing small-scale phenomena or sharp gradients in time and space (Privé and Errico 2016). One of the important distinctions between statistical interpolation methods like kriging and observational data assimilation methods (discussed previously) is that kriging

TABLE 1. Summary of spatial (horizontal and vertical) and temporal autocorrelation scales referenced in the text based upon correlation thresholds of 0.5, 0.37, or 0.2 for horizontal wind $|V_h|$, temperature T, water vapor, rainfall, rain rate, and vertical velocity w. Correlation length scales that were specifically for convective regions are denoted as "C," and nonconvective regions are denoted as "NC." Observation types (obs type) are listed, and the locations of the observations are noted for each referenced study. Observation types include surface (sfc stations), boat (boat stations), radio acoustic sounding system (RASS), satellite, lidar, S-band radar, or X-band radar.

Variable	Correlation	Vertical distance	Horizontal distance	Time	Obs type	Location	Reference
$\|V_h\|$	0.5	—	0–100 km	—	Sfc stations	Land	Wylie et al. (1985)
$\|V_h\|$	0.5	—	400 km	—	Boat stations	Ocean	Wylie et al. (1985)
$\|V_h\|$	0.5	—	—	4–6 h	Sfc stations	Land	Brett and Tuller (1991)
$\|V_h\|$	0.37	—	—	11 h (at 40 m)	RASS	Land	Pérez et al. (2004)
$\|V_h\|$	0.37	—	—	5 h (at 300 m)	RASS	Land	Pérez et al. (2004)
T	0.5	—	800–1000 km	—	Sfc stations	Land	Gunst (1995)
T	0.5	—	200–600 km	—	Satellite	Upper air	Nichol and Wong (2008)
T	0.37	—	—	7 h (at 40 m)	RASS	Land	Pérez et al. (2004)
T	0.37	—	—	8 h (at 140 m)	RASS	Land	Pérez et al. (2004)
T	0.5	—	—	12 h	Satellite	Over ITCZ	Raymond et al. (2003)
Water vapor	0.37	0.45 km (C)	—	—	Lidar	Airborne	Fisher et al. (2013)
Water vapor	0.37	0.2–0.3 km (NC)	—	—	Lidar	Airborne	Fisher et al. (2013)
Rainfall	0.5	—	4 km	—	Rain gauge	Land	Habib et al. (2001)
Rain rate	0.5	—	10 km (NC)	—	S-band radar	Land	Bringi et al. (2015)
Rain rate	0.5	—	4 km (C)	—	S-band radar	Land	Bringi et al. (2015)
Rainfall	0.5	—	1.5–4 km	—	Reports/radar	Land	Jameson (2017)
w	0.5	0.2–0.3 km	0.2–0.3 km	—	Lidar	Land	Lothon et al. (2006)
w	0.2	4–7 km	4–6 km	—	X-band radar	TC eyewall	Black et al. (1996)
w	0.2	2–4 km	1–4 km	—	X-band radar	TC rainband	Black et al. (1996)

is based completely on observations (Biau et al. 1999). Data assimilation is dependent on observations, and model physics, resolution, and domain size (e.g., Aberson 2008).

Temporal and spatial (both horizontal and vertical) variability of observations in various atmospheric phenomena suggest a complex relationship between the autocorrelation, observational density, observation method, and location of the observations. Table 1 summarizes the findings of studies that examined the temporal or spatial autocorrelations for horizontal wind speed $|V_h|$, T, water vapor, precipitation, and w. It is important to note that most of the studies presented in Table 1 did not analyze observations from TCs, evaluated various physical parameters and observations, used different instrumentation, studied a range of length scales, and used a range of critical correlation coefficients to determine autocorrelation scales. Nevertheless, they are included because of the lack of studies that have examined autocorrelations in TCs and they provide some context to the autocorrelations observed from the TCI dataset.

There are large variations in the autocorrelation horizontal distances for the non-TC variables considered in Table 1, with lengths ranging from 200 m (w; Lothon et al. 2006) to 1000 km (T; Gunst 1995). The vertical autocorrelation length scales for w and water vapor given in Table 1 are comparable and less than 1 km (Lothon et al. 2006; Fisher et al. 2013). The 0.5 autocorrelation temporal scales for T and horizontal wind speed (Table 1) are comparable, between 4 and 12 h, and are a function of altitude (Brett and Tuller 1991; Raymond et al. 2003; Pérez et al. 2004). Horizontal autocorrelation spatial scales for T are greater than, or comparable to, the horizontal autocorrelation spatial scales for horizontal wind (Table 1). Convection, and variables related to convection (e.g., precipitation rate), should have smaller correlation length scales horizontally due to higher small-scale variance (Fisher et al. 2013). Spatial autocorrelations in precipitation and rain rate drop below 0.5 from 1.5 to 10 km, with convective precipitation primarily at 4 km and stratiform precipitation generally at larger distances (Table 1). Lothon et al. (2006) examined the autocorrelation of w in the daytime, convective, planetary boundary layer (PBL) using Doppler lidar data and found small 0.5 autocorrelation distances between 200 and 300 m both horizontally and vertically (Table 1).

Black et al. (1996) examined the spatial autocorrelations of w in TCs from flight-level and Doppler radar data. They found that w autocorrelations of approximately 0.2 were statistically significant, horizontal and vertical autocorrelation distances were between 1 and 6 km, and updrafts were more spatially correlated than downdrafts, especially within the eyewall. The 0.2 autocorrelation threshold noted in Black et al. (1996) indicates statistically significant relationships, but does not indicate that the autocorrelation is strong. The use of

a higher autocorrelation threshold, like 0.5, would indicate a stronger relationship and decrease the horizontal, and vertical, autocorrelation distances in Black et al. (1996) by approximately 50%.

The definition of convection, updrafts, and downdrafts is also important in discerning the autocorrelation scales within updrafts and downdrafts. Jorgensen et al. (1985) defined convective vertical motions in TC flight-level data as continuous positive or negative vertical velocities for at least 500 m, with at least one data point achieving a magnitude of $0.5\,m\,s^{-1}$. Convective cores were defined as continuous w magnitudes of at least $1\,m\,s^{-1}$ for 500 m or greater. These distances and values were determined iteratively and subjectively in LeMone and Zipser (1980) to more easily differentiate turbulent motions from coherent vertical velocities without needing a complex statistical analysis. This definition was also adopted by studies such as Black et al. (1994); however, the spatial correlations of the w data were not presented. Black et al. (1996) defined an updraft or downdraft as continuous, X-band radar, vertical velocities exceeding $|1.5\,m\,s^{-1}|$ with at least one data point exceeding $|3\,m\,s^{-1}|$.

Eastin et al. (2002a,b, 2005) examined the spatio-temporal characteristics and statistics of instrument wetting events (IWEs) in TCs, which are periods where flight-level, probe-derived temperature measurements were significantly [using the 3σ (std dev) level; or $\Delta T = 0.5$°C] colder than radiometer-derived temperatures. These IWEs were primarily correlated with the presence of updrafts and appreciable cloud water. The results from Eastin et al. (2002a,b, 2005) are not included in Table 1, because they did not directly report upon the autocorrelation of the data nor present correlograms of the data. Eastin et al. (2002a) showed that 90% of the IWEs were less than 10 km in scale. Magnitudes of moisture, w, and ΔT decrease and, therefore, decorrelate rapidly within 3–6 km of the peak of the IWEs (Eastin et al. 2002a). Equivalent potential temperature θ_e and moisture values decreased rapidly (decorrelated) within 8 km radially outward of updraft maxima (Eastin et al. 2002b). The mean IWE diameters were also a function of altitude, where IWE diameters were 7 km below the freezing level and 14 km above (Eastin et al. 2002a).

In this study, an analysis is conducted to evaluate the temporal and spatial autocorrelations of the XDDs used in TCI with the kriging spatial interpolation framework. The autocorrelation of data points in individual soundings, as well as the spatial correlation between adjacent soundings, are considered. In section 2, the data and methods used are described. Section 3 shows the results of the temporal and spatial autocorrelations.

TABLE 2. List of the minimum, maximum, mean, and median dropsonde spacing for each day to the nearest kilometer.

Day	Name	Min	Max	Mean	Median
27 Sep	Marty	6	44	18	17
28 Sep	Marty	3	83	21	13
2 Oct	Joaquin	7	150	39	41
3 Oct	Joaquin	5	344	54	38
4 Oct	Joaquin	8	120	37	27
5 Oct	Joaquin	9	121	33	28
20 Oct	Patricia	18	267	87	44
21 Oct	Patricia	7	69	26	24
22 Oct	Patricia	4	142	26	11
23 Oct	Patricia	3	73	22	25

Conclusions are drawn in section 4 and a discussion of the results, and their implications for future dropsonde studies, is provided.

2. Data and methods

Three of the primary goals of TCI were to 1) document the horizontal, and vertical, structure of the outflow layer and the inner core of TCs; 2) understand the role of the TC outflow layer on intensity change and how it couples with convection; and 3) examine the impact of assimilating observations of the outflow layer and TC core on track, and intensity, forecasts. A total of 140, 328, and 257 XDDs were launched into Marty (27–28 September), Joaquin (2–5 October), and Patricia (20–23 October), with most flights being transects over the TC centers or figure-four patterns over a duration of 1–2 h. The minimum, maximum, mean, and median sounding spacing for each day are provided in Table 2. The temporal and spatial autocorrelations were computed for w, $|V_h|$, T, and θ_e.

Adjacent data points in time and space with correlations above 0.5 are considered highly correlated (Brooks and Carruthers 1978). The statistical significance of the autocorrelations is estimated by 95% confidence levels. Autocorrelations above 0.5 are statistically significant well above the 95% confidence level in both time and space for all variables in the dataset (not shown) and, therefore, indicate both strong and statistically significant autocorrelations.

Autocorrelation distances and times below the spatial and temporal resolution of the dataset are interpolated estimates limited by the spacing and number of observations. In such a situation, it can be confidently stated that the autocorrelation threshold is below the median resolution, but the exact autocorrelation distance or time cannot be verified or confidently stated. Further, any apparent variance in autocorrelation thresholds that are below the median sounding spacing from day to day or storm to storm also cannot be verified or confidently

stated. These distances and times are still valuable, however, to estimate the temporal and spatial resolutions required to sample TCs from transects of soundings. The spatial autocorrelation estimates in particular, are presented and discussed in this study, with the understanding that the exact values are estimated and may not be fully conclusive.

The vertical velocities, TC centers, and RMWs were obtained following the methodology of Nelson et al. (2019). The same data restriction methods used in Nelson et al. (2019) were employed in this study to ensure that autocorrelations were computed for the same subset of the TCI data. Data were restricted to only include data points for dropsondes that terminated at an altitude below 500 m to ensure that data were recorded in the low levels of the TCs, comparable to Stern et al. (2016). Data points that occurred outside of a radius of 10 times the RMW ($10R^*$; Nelson et al. 2019) were also removed, which corresponds to a range of radii from 112 to 768 km depending on the date. The $10R^*$ restriction was used to ensure that data points outside of the TCs themselves (i.e., environmental soundings) were removed. The results of this study, however, are not sensitive to the inclusion of data beyond $10R^*$, with spatial autocorrelation scales differing by 1–2 km at most when removing the $10R^*$ radial restriction, and temporal autocorrelation scales differing by less than 1 s. Data were also restricted to only use points below an altitude of 17.5 km, as upon launching from an altitude of 19 km, the dropsondes take time to adjust to the ambient air (~0.5–1 km; Nelson et al. 2019). A total of 437 dropsondes (276 659 data points) were used in this study after the above data restrictions. The raw "level 1" sounding data were used in this study in lieu of the quality-controlled TCI dropsonde dataset documented by Bell et al. (2016) to ensure that the autocorrelation scales observed were associated with the data itself and not from filtering techniques. Similar to Nelson et al. (2019), all data used in this study were at 1-Hz resolution, which is coarser than the native 2- or 4-Hz data acquisition frequency.

To compute the temporal and spatial autocorrelation scales, the data within any sounding need to be detrended (Janert 2011). If a trend or mean state is present in the data, then correlograms show smoothed and high-amplitude periodic curves or large, negative correlations at long lags (see the online supplemental material). Rather than using a linear detrend, median atmospheric profiles of w, T, $|V_h|$, and θ_e were used to detrend the data. Six detrend methods were explored: 1) no detrend, 2) detrend using median profiles from a specific date (date detrend), 3) detrend using median profiles from a specific TC (storm detrend), 4) detrend using median profiles from the entire dataset (total detrend), 5) detrend using median profiles within four radial sections from the entire dataset (radial detrend), and 6) detrend using median profiles within four radial sections from a specific date (D+R detrend). The sixth method (D+R detrend) was ultimately used in this study, because it exhibited the largest autocorrelations among the most parameters, while accounting for the variance in the mean state radially, from date to date, and from storm to storm. The four radial sections were 1) $\leq 1.25R^*$, 2) $1.25R^*$–$3R^*$, 3) $3R^*$–$5R^*$, and 4) $5R^*$–$10R^*$. Note that, by combining all soundings within $1.25R^*$, data from the high-gradient region near the eyewall are used and the median state can be influenced by the soundings within the eye itself. Further details about the six detrending methods, their results, and comparisons can be found in the online supplemental material.

The D+R detrend median profiles for each variable and each date are provided in Figs. 1–3 and the total number of soundings in each radial section are provided in Table 3. The mean and median number of soundings in each radial section was 11–12, with a maximum of 24 (Joaquin on 5 October) and a minimum of zero (Patricia on 20 October). Many of the median w profiles resemble profiles observed by Black et al. (1996) and primarily show weak, near-zero vertical motions below the average freezing level (5–6 km) and stronger vertical velocities aloft (Figs. 1a–d, 2a–d, and 3a–d), but it is unknown if this increase is real or due to errors aloft (Nelson et al. 2019). The median w profiles were especially noisy in Patricia on 20 and 23 October likely due to the small number of soundings in the radial section (Table 3) or strong vertical motions in the eyewall (Nelson et al. 2019). The $|V_h|$ median profiles differ from day to day and show the evolution of the TC wind field, but also show that peak $|V_h|$ strengths generally occurred between 0.5 and 1 km (Figs. 1e–h, 2e–h, and 3e–h). The $|V_h|$ median profile for Patricia on 23 October had a noisy double jet structure, with strong median $|V_h|$ from 5 to 7 km similar to the double jet structure in the eyewall of Patricia shown by Rogers et al. (2017) (Fig. 3e). T and θ_e varied slightly from day to day, and had smooth decreases aloft for T and increases aloft for θ_e (Figs. 1i–l, 2i–l, and 3i–l).

To calculate horizontal dropsonde-to-dropsonde autocorrelations, median profiles similar to those in Figs. 1–3 were created using 0.25-km bins from 0 to 17 km height to account for small altitudinal variations among the observations and differences in the number of data points in each sounding. The bin size was chosen to match the altitudinal binning scheme by Nelson et al. (2019). Spatial dropsonde-to-dropsonde autocorrelations and corresponding distances were computed using the following equations:

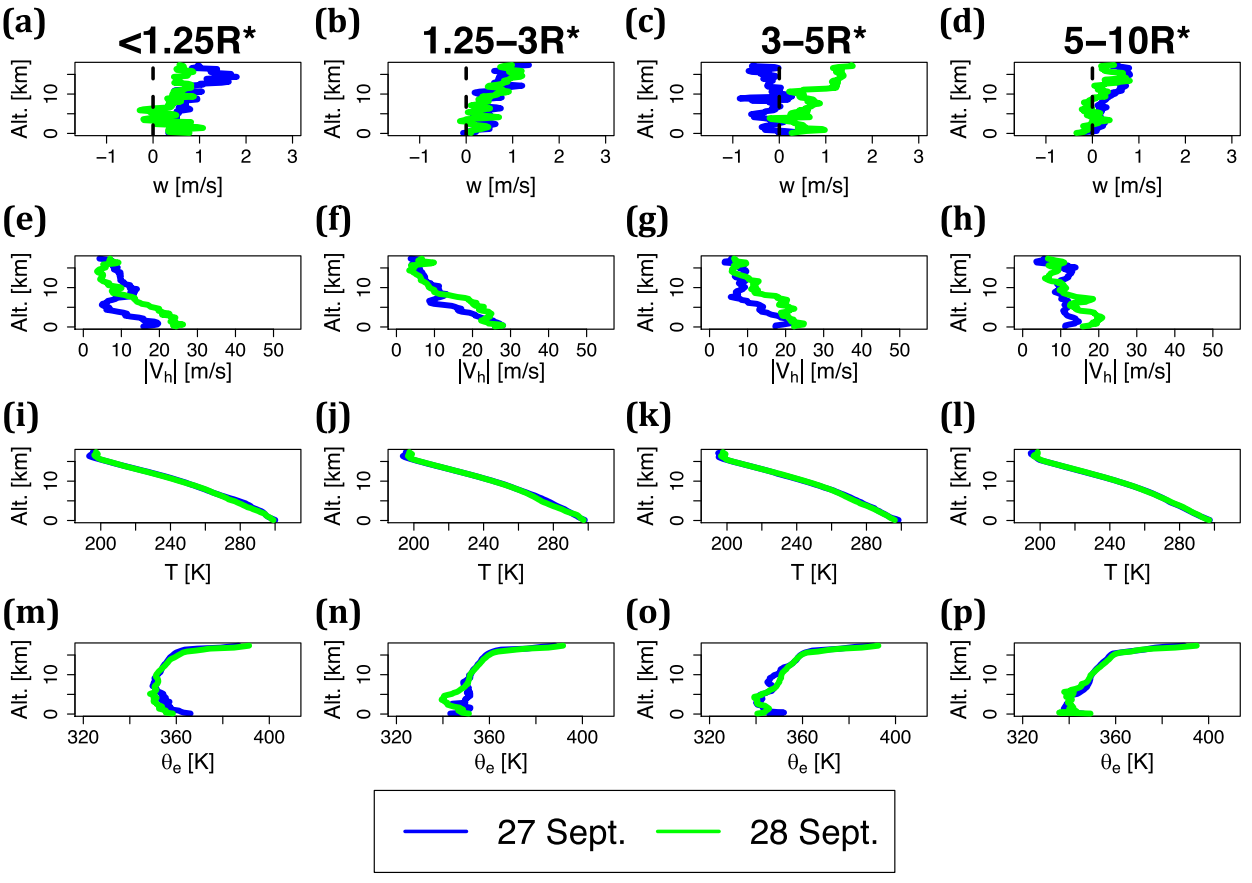

FIG. 1. Median atmospheric profiles of (a)–(d) w (m s^{-1}), (e)–(h) $|V_h|$ (m s^{-1}), (i)–(l) T (K), and (m)–(p) θ_e (K) during Marty for data (left) within 1.25R*, (left center) between 1.25R* and 3R*, (right center) between 3R* and 5R*, and (right) between 5R* and 10R*.

$$\overline{r_t}(k) = \frac{\sum_{i=1}^{n} (X_i' - \overline{X_i'})(X_{i+k}' - \overline{X_{i+k}'})}{\sqrt{\sum_{i=1}^{n} (X_i' - \overline{X_i'})^2 (x_{i+k}' - \overline{X_{i+k}'})^2}} \quad \text{and} \quad (1)$$

$$d = \overline{\sqrt{(x_i - x_{i+k})^2 + (y_i - y_{i+k})^2}}, \quad (2)$$

where the autocorrelation $\overline{r_t}$ is calculated for the binned, median, D+R detrended data (X') at a distance d in the x–y plane. The autocorrelation of each sounding is calculated from pairs of all soundings and not just those immediately adjacent to a given sounding. n is the total number of soundings for each date or TC, and k is an index that runs from 0 to $n - 1$ that accounts for each sounding in the calculation. If it is assumed that the D+R detrend process accurately removed the mean state in each sounding, then the mean of X' should be zero in all of the equations presented here. The d used is the mean distance between the two soundings. Given the uneven spacing of soundings and the finer resolution of observations within the core, the spatial autocorrelation distances presented here may be biased toward lower values. In contrast, the use of a median profile creates smoother soundings than what was actually observed in TCI and may bias autocorrelation distances toward larger values. These assumptions in the methodology, however, do not severely impact the results of the study, because statistically significant high autocorrelations are not expected at large (>100 km) distance scales within a TC.

To calculate the autocorrelations within an individual sounding, data were ordered with respect to time and the "acf" function in the R software package was used for each individual sounding, for each observation day, and for each storm. The acf function computes autocorrelation using the following equations:

$$r_t = c_t / c_o, \quad (3)$$

$$c_t = \frac{1}{n} \sum_{\min(n-t,n)}^{\max(1,-t)} [X_{s+t}' - \overline{X'}][X_s - \overline{X'}], \quad \text{and} \quad (4)$$

$$c_o = \frac{1}{n} \sum [X' - \overline{X'}]^2, \quad (5)$$

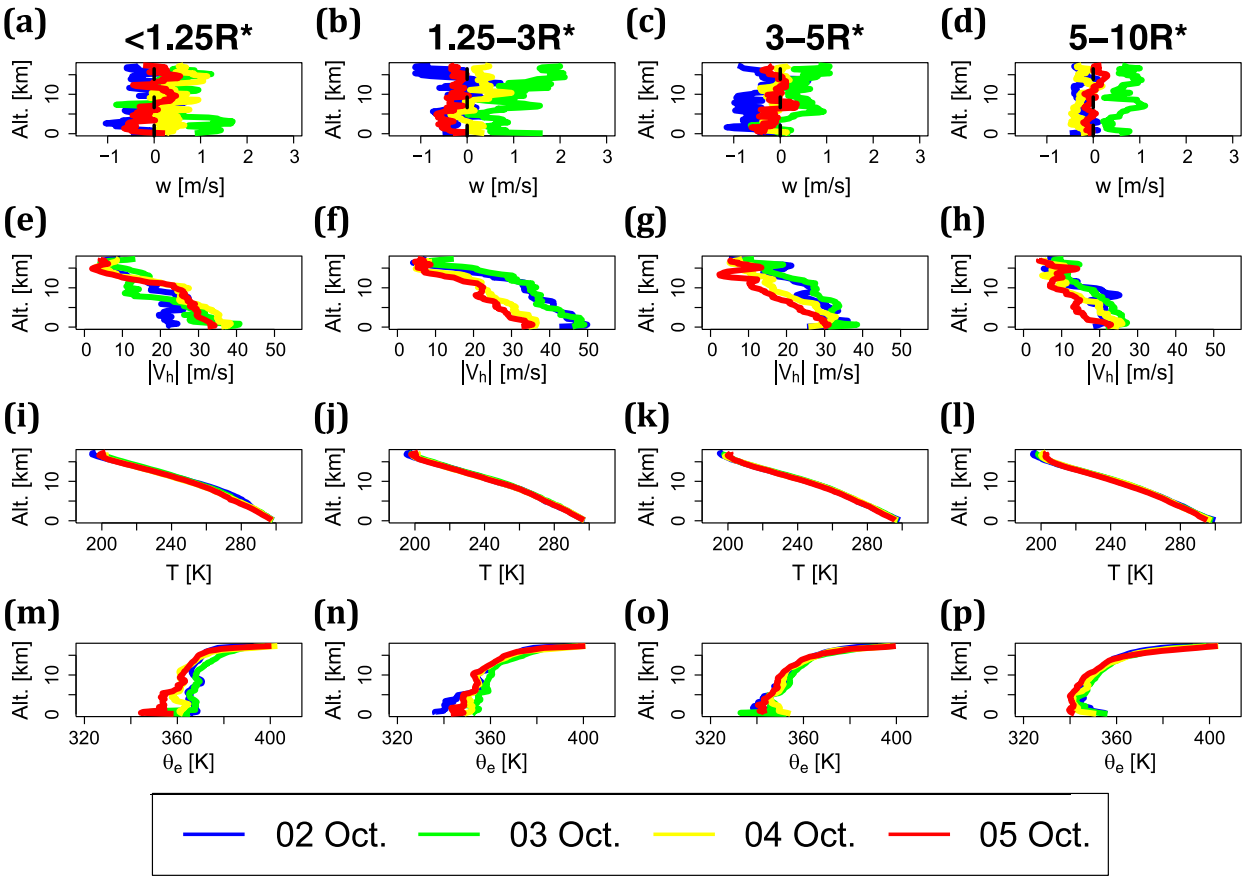

FIG. 2. As in Fig. 1, but for Joaquin.

where r_t is the autocorrelation, c_t is the autocovariance, c_o is the variance of the series, n is the length of the series, s is time, and t is some lag forward in time (Venables and Ripley 2002). For the temporal autocorrelations within any given sounding, the X' data were not binned like in the dropsonde-to-dropsonde data. The soundings, therefore, have differences in the total number of data points, which is a function of the fall speed, horizontal wind speed, dropsonde fall behavior, and missing data. The autocorrelations were computed assuming that no missing data were present and the temporal resolution was 1 Hz. If there were missing data in the sounding, the data were not replaced with an interpolated mean value or padded with a fill value, because that would, potentially, increase the autocorrelations artificially depending on the number of missing data points. It is hypothesized that missing data would affect the results by biasing the autocorrelations to smaller temporal scales.

Because of the highly accurate data telemetry, however, large regions of missing data were rarely present in soundings. The total percent of missing data points is negligibly small for the soundings considered, after altitude and radial restriction, at 5%. Most regions of missing data occur over depths of less than 100 m. The autocorrelation scales and correlograms presented in this study are interpolated splines over all of the soundings for an individual date or TC, which would decrease the impact of missing data in a relatively small number of soundings within the dataset.

3. Results

The autocorrelations for each TC and in total were plotted as correlograms. Individual correlograms for each of the 10 days in the dataset are not provided, but the results from those figures are summarized in Tables 4 and 5, and Fig. 4. Correlograms for each TC are provided in Figs. 5 and 6. The correlograms are smoothed splines fitted to scatterplots of the correlograms for each sounding or altitude level. Table 4 documents the autocorrelation spatial scales where correlation drops below 0.5 for adjacent data points at a fixed altitude (dropsonde to dropsonde). Table 5 documents the autocorrelation time scales where correlation drops below 0.5 for data within a given individual sounding.

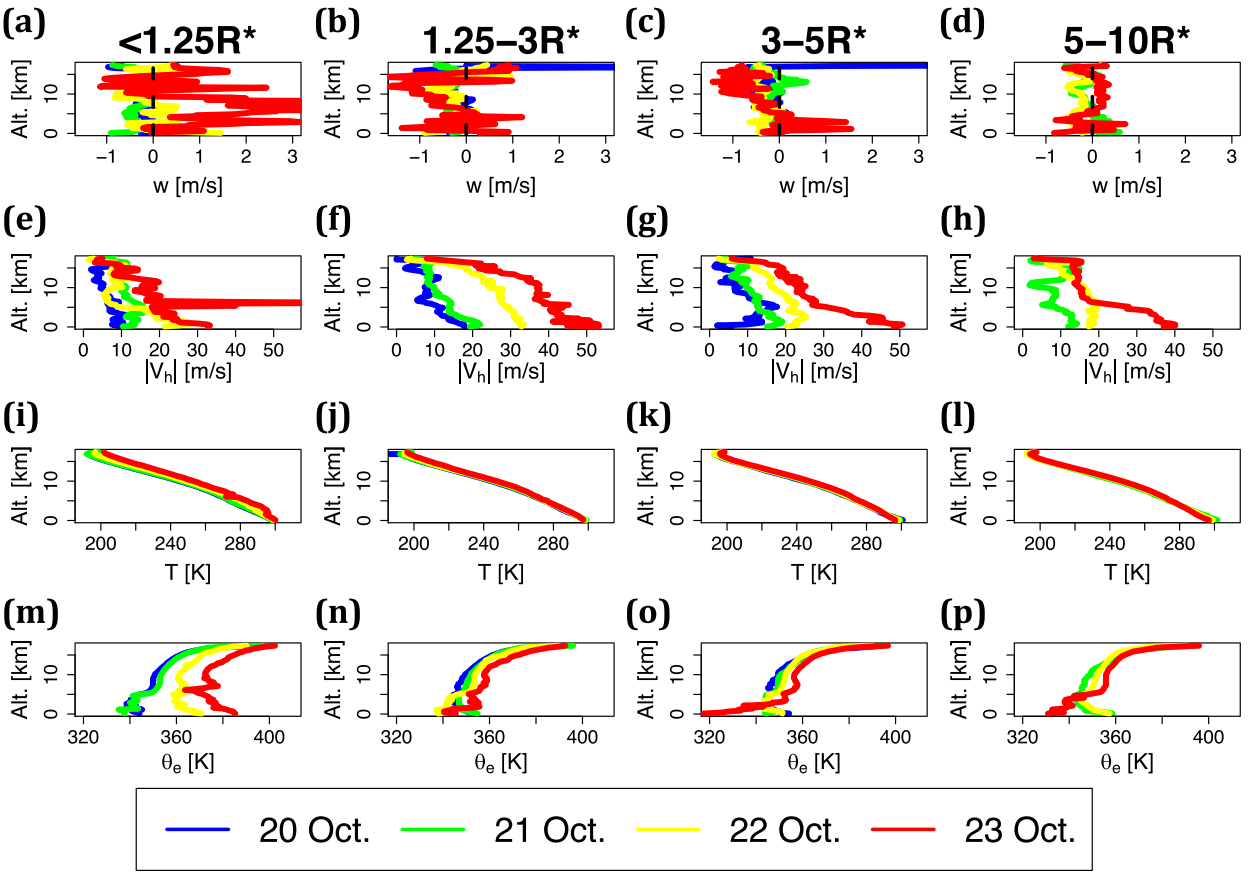

FIG. 3. As in Fig. 1, but for Patricia.

The means, medians, and standard deviations for the spatial and temporal autocorrelation scales computed from all 10 observation days are included in Tables 4 and 5.

a. Correlations from dropsonde to dropsonde

All of the calculated daily spatial autocorrelation length scales were below the mean and median sounding spacings, and were comparable to, or less than, the minimum observed sounding spacings (Tables 2 and 4). The data from Table 4 imply that the actual spatial autocorrelation length scales were below the median spacing, but the exact values cannot be verified with the observed dataset. The values discussed below and presented in Table 4, therefore, are rough estimates.

Vertical velocity and θ_e had relatively small mean and median spatial autocorrelation scale estimates at 4–6 km (Table 4), with w generally being the smallest. All variables had comparable standard deviations in the estimated spatial autocorrelation scales between 4 and

TABLE 3. List of the number of dropsondes within each of the four radial sections and in total on each day.

Day	Name	≤1.25R*	1.25R*–3R*	3R*–5R*	5R*–10R*	Total
27 Sep	Marty	11	13	6	20	50
28 Sep	Marty	13	16	15	14	58
2 Oct	Joaquin	15	13	6	10	44
3 Oct	Joaquin	11	11	7	14	43
4 Oct	Joaquin	13	16	15	11	55
5 Oct	Joaquin	9	13	7	24	53
20 Oct	Patricia	5	5	2	0	12
21 Oct	Patricia	13	18	13	7	51
22 Oct	Patricia	5	13	12	13	43
23 Oct	Patricia	5	6	9	8	28

TABLE 4. List of dropsonde-to-dropsonde spatial 0.5 autocorrelation thresholds, or estimated thresholds, (km) for each day in the dataset for vertical velocity w, horizontal wind speed $|V_h|$, temperature T, and equivalent potential temperature θ_e. The size of the RMW (km) and TC intensity ($m\,s^{-1}$) are also noted.

Day	Name	w	$\lvert V_h\rvert$	T	θ_e	RMW	Intensity
27 Sep	Marty	5	10	7	7	37	26
28 Sep	Marty	4	7	5	4	21	36
2 Oct	Joaquin	4	7	5	5	31	57
3 Oct	Joaquin	3	5	5	3	27	67
4 Oct	Joaquin	5	19	15	8	38	44
5 Oct	Joaquin	5	12	7	5	49	39
20 Oct	Patricia	17	15	16	18	77	15
21 Oct	Patricia	5	16	14	5	40	26
22 Oct	Patricia	4	13	9	4	19	59
23 Oct	Patricia	1	7	2	1	11	93
Mean	—	5	11	9	6	35	46
Median	—	4	11	7	5	34	41
Std dev	—	4	5	5	5	18	22

TABLE 5. As in Table 4, but for the temporal 0.5 autocorrelation thresholds (s) for each day in the dataset and any given individual sounding. The size of the RMW (km) and TC intensity ($m\,s^{-1}$) are also noted.

Day	Name	w	$\lvert V_h\rvert$	T	θ_e	RMW	Intensity
27 Sep	Marty	19	25	22	28	37	26
28 Sep	Marty	23	31	24	31	21	36
2 Oct	Joaquin	23	41	27	25	31	57
3 Oct	Joaquin	25	38	35	34	27	67
4 Oct	Joaquin	22	31	23	31	38	44
5 Oct	Joaquin	20	31	21	30	49	39
20 Oct	Patricia	8	21	15	19	77	15
21 Oct	Patricia	22	32	13	22	40	26
22 Oct	Patricia	21	27	17	25	19	59
23 Oct	Patricia	20	33	17	20	11	93
Mean	—	20.3	31.0	21.4	26.5	35	46
Median	—	21.5	31.0	21.5	26.5	34	41
Std dev	—	4.4	5.5	6.1	5.1	18	22

5 km, but $|V_h|$ and T had the smallest spreads (Table 4). Estimated mean and median $|V_h|$ and T spatial autocorrelation scales were 10–11 and 7–9 km, respectively (Table 4).

The estimated spatial 0.5 autocorrelation scales for all variables increased with increasing RMW (Fig. 4a). The spatial scales for w and θ_e had the strongest positive correlations with RMW size. While the correlations do not indicate a robust, conclusive relationship between the RMW and spatial 0.5 autocorrelation scales because of the relatively small sample size and relatively large median sounding spacing, it is plausible that the spatial autocorrelation scales could be influenced by the storm-scale structure of the TCs. The $|V_h|$ and T do show appreciably strong (>0.5) correlations with the RMW, but not as strong as the other two variables. This result is interesting, because $|V_h|$ and T would be expected to have the strongest correlations with the RMW based upon the well-recognized idea that gradient or thermal wind balance dominates the storm-scale structure of TCs (e.g., Willoughby 1990; Molinari et al. 1993). Rather, variables associated with convective features (w and θ_e) are more correlated with the RMW. Figure 4a also illustrates that most of the estimated spatial scales are smaller than the RMW by a factor of 4–8, with $|V_h|$ mostly on the low end and w on the high end of the range. Despite the relationship between the RMW and autocorrelation length scales, data are still grouped by each TC to examine the differences in the temporal and spatial autocorrelations present from storm to storm.

Figure 5 shows the spatial correlograms for all four variables in Marty, Joaquin, and Patricia. Here, w and θ_e decorrelate rapidly within 10–20 km, reaching zero at approximately 20 km (Figs. 5a,d); T and $|V_h|$ decorrelate slower, reaching zero between 40 and 60 km (Figs. 5b,c). All of the variables have autocorrelations that fluctuate around zero outside of 50 km (Fig. 5). The median sounding spacing when data are grouped by each TC is, approximately, 11–14 km. The 0.5 autocorrelation length scales were generally smaller than the median sounding spacing by a factor of 3–5 for all variables in all three TCs. All three TCs had horizontal autocorrelation length scale estimates between 3 and 4 km, depending upon the variable considered (Fig. 5). These spatial autocorrelation scales differ from the daily autocorrelation scale estimates, and are less than the mean and median estimated scales in Table 4, because Fig. 5 shows the spatial autocorrelation composited from data in each of the three TCs. The spatial autocorrelation scales were examined as a function of altitude, but the corresponding distances were often nonlinear or nonmonotonic and no robust conclusions could be made.

To put the estimated spatial autocorrelation scales into context, the values are compared to the correlation length scales in Table 1. The correlation distances observed in non-TC studies, except for w, are considerably larger compared to what was observed in the TCI data. For example, the estimated spatial autocorrelation scales for T observed on an individual day and in an individual TC are much smaller than the horizontal autocorrelation distances observed by Gunst (1995) and Nichol and Wong (2008). This finding is robust, even when considering the median sounding spacing. The estimated spatial autocorrelation scales for w were primarily between 1 and 5 km from day to day (excluding 20 October), and 2 and 4 km from storm to storm (Table 4 and Fig. 5a). The w estimated spatial autocorrelation scales are most comparable to the rainfall and convective rain rate autocorrelation distances over land with rain gauge, and

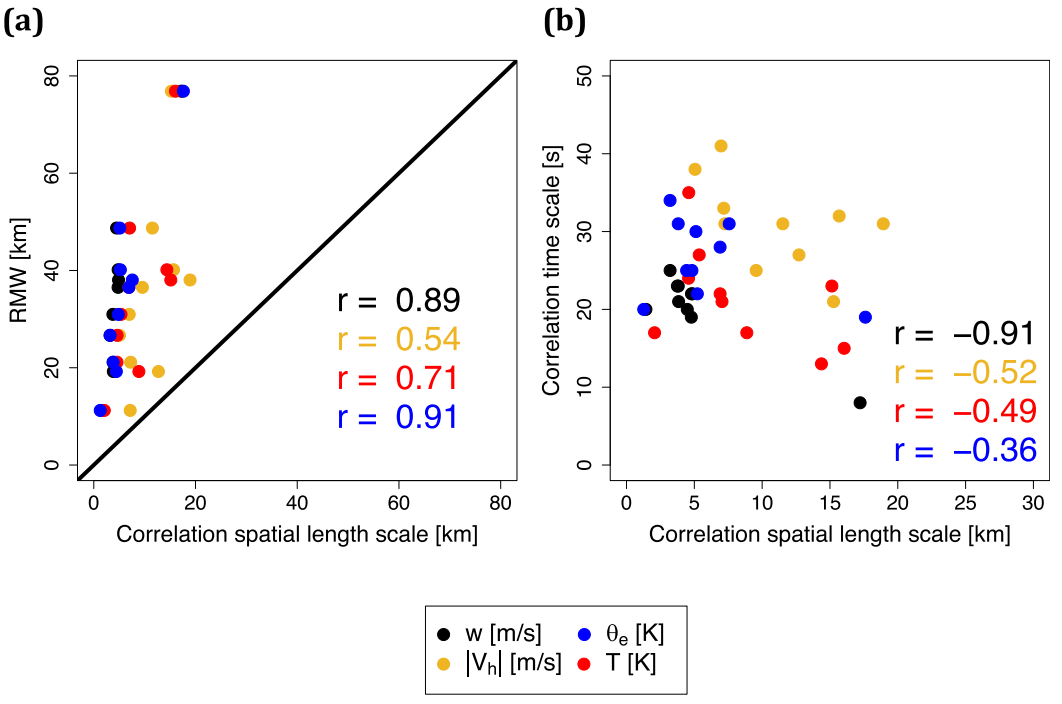

FIG. 4. Comparison of the (a) daily dropsonde-to-dropsonde spatial autocorrelation scales (km) with the RMWs (km) and (b) daily dropsonde-to-dropsonde spatial autocorrelation scales with the daily temporal 0.5 autocorrelation length scales (s) for w, T, $|V_h|$, and θ_e (black, red, orange, and blue, respectively). The 1:1 (or $x = y$) line (black) is shown in (a).

radar, data in Habib et al. (2001), Bringi et al. (2015), and Jameson (2017). The estimated spatial autocorrelation scales are also slightly smaller than the w 0.2 autocorrelation length scales adjacent to updrafts and downdrafts in TCs as shown by Black et al. (1996), but are comparable if Black et al. (1996) used a 0.5 autocorrelation threshold. The differences between this study and Black et al. (1996) may not be robust, however, considering that the 0.5 autocorrelation spatial scales are smaller than the median sounding spacing.

b. *Correlations within a sounding*

The temporal 0.5 autocorrelation scales were above 8 s for all variables and for each observation day, with most above 15 s (Table 5). Mean and median temporal autocorrelation scales ranged from 20 to 31 s for all variables (Table 5). The smallest mean and median temporal scales were for w and T. The smaller temporal autocorrelation thresholds in T and w could be due to smaller thermal perturbations away from the median profiles in each radial section (e.g., Fig. 2) and weaker vertical motions dominating the vertical velocity distribution (Nelson et al. 2019). The mean and median temporal autocorrelation scales for θ_e were slightly larger than for w and T at 26.5 s. The $|V_h|$ had the largest temporal autocorrelation scales within individual soundings at approximately 30 s. The estimated still air dropsonde fall speed ranges from approximately 52 m s^{-1} at 17.5 km to 18 m s^{-1} at sea level (Nelson et al. 2019). It is estimated from the typical fall speeds that vertical autocorrelation length scales would likely range from 0 to 2 km.

Figure 4b shows that as the horizontal autocorrelation length scale increases, the temporal autocorrelation scale generally decreases for w, $|V_h|$, and T. The θ_e temporal scales have a weak, negative correlation with the horizontal autocorrelation length scales, but this is primarily due to one outlier data point. If this data point was removed, the correlation would be positive at 0.32. This single data point outlier is not present in the other three variables, but occurred in Patricia on 20 October, where few dropsondes were launched (Table 3). The strongest correlation was for the w temporal and spatial autocorrelation scales at −0.91. The general negative correlation, especially for w, is not surprising. As a hypothetical situation, if an XDD sampled a coherent feature through the depth of the troposphere, like an eyewall updraft, that sounding will likely not correlate well with other dropsonde data launched outside of the convective region of the eyewall, leading to smaller spatial correlation scales. Conversely, if an XDD

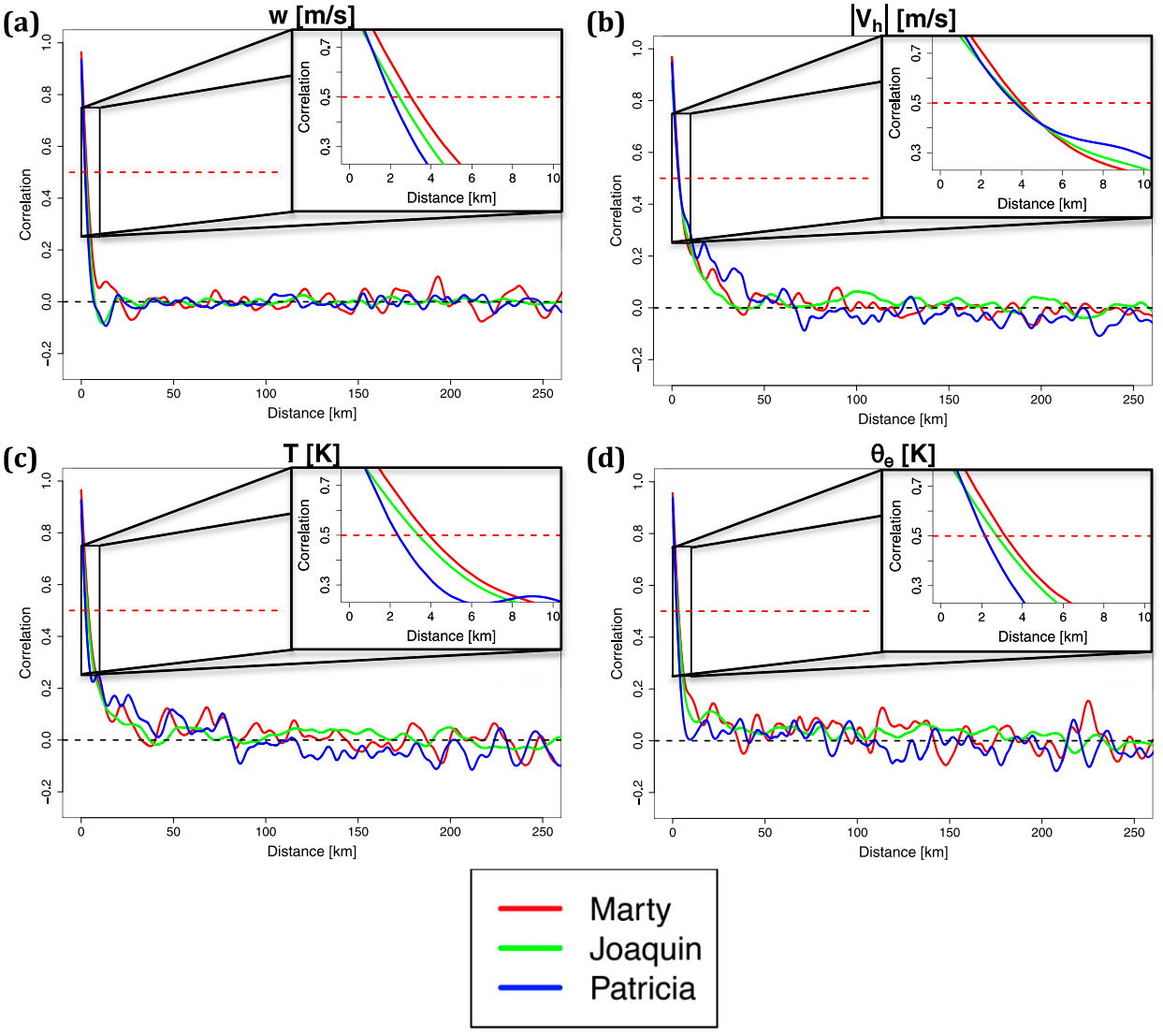

FIG. 5. Spatial autocorrelations for XDDs launched into Marty (red), Joaquin (green), and Patricia (blue) for for (a) w, (b) $|V_h|$, (c) T, and (d) θ_e. Correlations of 0.5 and 0.0 are denoted with dashed red and black lines, respectively. Each panel has an inset in the upper-right corner that shows the variations in the 0.5 autocorrelation crossings.

sampled an area with weak radial gradients, and incoherent vertical structure, then the dropsonde-to-dropsonde spatial scale will be larger and the temporal scale will be smaller. Similar to the relationship between the RMW and spatial 0.5 autocorrelation scale (Fig. 4a), these correlations do not provide robust conclusions because of the relatively small sample size, but they can be used to develop a hypothesis as to the relationships between the two scales.

Figure 6 shows the temporal correlograms for all four variables in Marty, Joaquin, and Patricia. All variables decorrelate rapidly within 80 s, reaching zero at approximately 100–150 s (Fig. 6). Weak, negative autocorrelation values were observed at longer time lags for all variables (Fig. 6). w decorrelated the fastest, but the difference in the rate of decorrelation is negligible.

Joaquin consistently had the largest 0.5 autocorrelation temporal scales out of the three TCs for all variables, but both Marty and Joaquin had the same temporal 0.5 autocorrelation scales for θ_e (Fig. 6d). There was little variation in the temporal 0.5 autocorrelation scales for w from storm to storm, with temporal scales of 19–21.5 s (Fig. 6a). Marty and Patricia had comparable 0.5 autocorrelation temporal scales for $|V_h|$ (27–28.5 s). In comparison, the 0.5 autocorrelation temporal scales for $|V_h|$ in Joaquin were approximately 33 s. Patricia had considerably smaller temporal autocorrelation scales for T and θ_e when compared with Marty or Joaquin. The 0.5

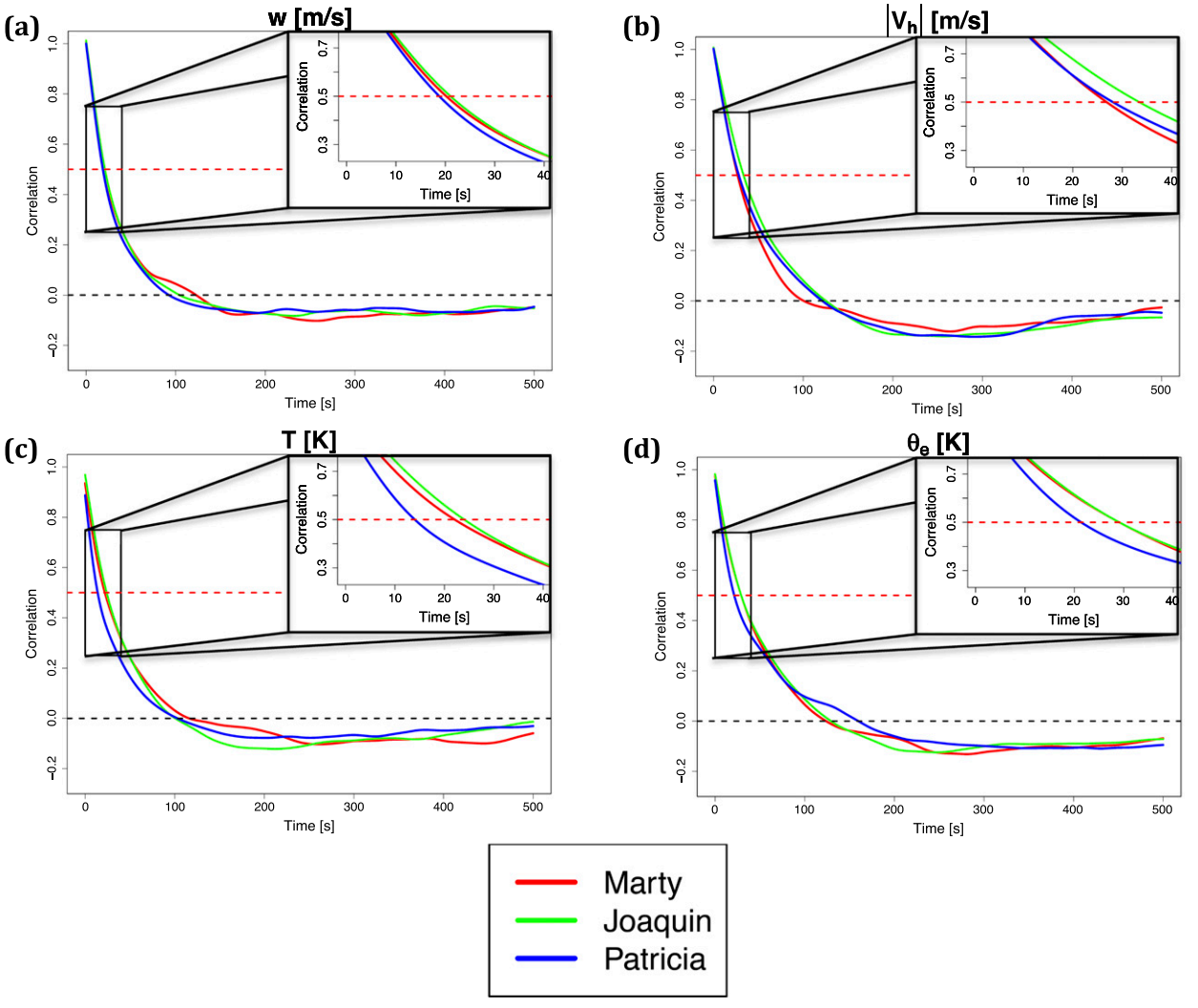

FIG. 6. As in Fig. 5, but for temporal autocorrelations in each sounding.

autocorrelations were also examined as a function of radius, but the corresponding temporal scales were often nonlinear or nonmonotonic and no robust conclusions could be made.

c. *Correlations within updrafts and downdrafts*

Given that the typical structure of a TC features strong kinematic and thermal perturbations within the convective eyewall and rainbands, it is possible that the 0.5 autocorrelation temporal scales differ in soundings that observed updrafts or downdrafts from soundings in less convective areas. It is also possible that the temporal scales in these updraft and downdraft soundings differ from the findings in Fig. 6 and Table 5, which include all soundings in the dataset. Updrafts and downdrafts are defined here following Nelson et al. (2019) as consecutive w above $\pm 2\,\mathrm{m\,s^{-1}}$ with at least one data point above $\pm 4\,\mathrm{m\,s^{-1}}$. There was not a requirement for the minimum depth for the updrafts or downdrafts. Updraft and downdraft soundings are the subset of soundings with at least one updraft or downdraft, respectively, in the sounding. The number of updraft and downdraft soundings for each day is provided in Table 6. In the situation where both an updraft and a downdraft is observed in a given sounding, it is classified as both an updraft and downdraft sounding. Soundings that contain both an updraft and a downdraft compose 3% of the entire dataset. Approximately 17% of the updraft soundings contain at least one downdraft, and approximately 35% of the downdraft soundings contain at least one updraft. The p values of below 0.05 are used to define statistically significant differences.

As an example, shown in Figs. 7 and 8 are sounding profiles from the eyewall of Patricia on 23 October.

TABLE 6. Number of updraft (U) and downdraft (D) soundings for each day.

Day	Name	U	D
27 Sep	Marty	4	3
28 Sep	Marty	9	5
2 Oct	Joaquin	13	15
3 Oct	Joaquin	15	4
4 Oct	Joaquin	4	0
5 Oct	Joaquin	5	0
20 Oct	Patricia	8	1
21 Oct	Patricia	5	1
22 Oct	Patricia	3	2
23 Oct	Patricia	12	6
Total	—	78	37

The red lines denote the start and end of the updraft following the definition of Nelson et al. (2019). The updraft occurred in the midlevels, was approximately 7.5 km deep, and was sampled for over 400 s (Figs. 7, 8). The updraft was also collocated with the midlevel jet shown by Rogers et al. (2017), a relatively warm θ_e bubble, and small variations in the T profile. The perturbation profile of T, however, shows strong, negative 5–10-K perturbations, and the perturbation profile of θ_e shows weak, near-zero perturbations in the middle of the updraft and strong, negative perturbations at the base of the downdraft (Figs. 9c,d). These perturbation profiles are not consistent with what is expected for an updraft sounding and may be due to the median profiles reflecting the relatively warmer low- and midlevel eye. In contrast, the w and $|V_h|$ perturbation profiles exhibited strong, positive perturbations within the defined updraft as expected for an eyewall updraft (Figs. 9a,b). The temporal autocorrelations within this sounding were significantly larger than for the entire date, with a p value of 0.009 (Fig. 10). The autocorrelations for the Patricia eyewall sounding ranged from approximately 70 s (w) to 120 s (θ_e).

Temporal autocorrelations were computed for all 78 updraft and 37 downdraft soundings on each day and are provided in Tables 7 and 8. The mean and median 0.5 autocorrelation temporal scales in updraft soundings were larger than, or comparable to, the temporal scales in all soundings, but the differences were not significantly different by Student's t tests (Tables 5, 7). Similarly, mean and median 0.5 autocorrelation temporal scales in downdraft soundings were larger than, or comparable to, the temporal scales in all soundings (Tables 5, 8). None of the differences, however, were statistically significant.

Figures 11 and 12 show the temporal autocorrelations for individual soundings computed similarly to the single sounding in Fig. 10. The temporal scales for w, $|V_h|$, T, and θ_e in updraft soundings have positive correlations with the maximum updraft depth in the soundings (Fig. 11). The correlation for w was strong at 0.76, with a p value of 6×10^{-16} (Fig. 11a). Correlations were also statistically significant at a p value below 0.05 for $|V_h|$ (0.04) and θ_e (0.008), but the correlations themselves are relatively weak compared to w. The positive, statistically significant correlations between

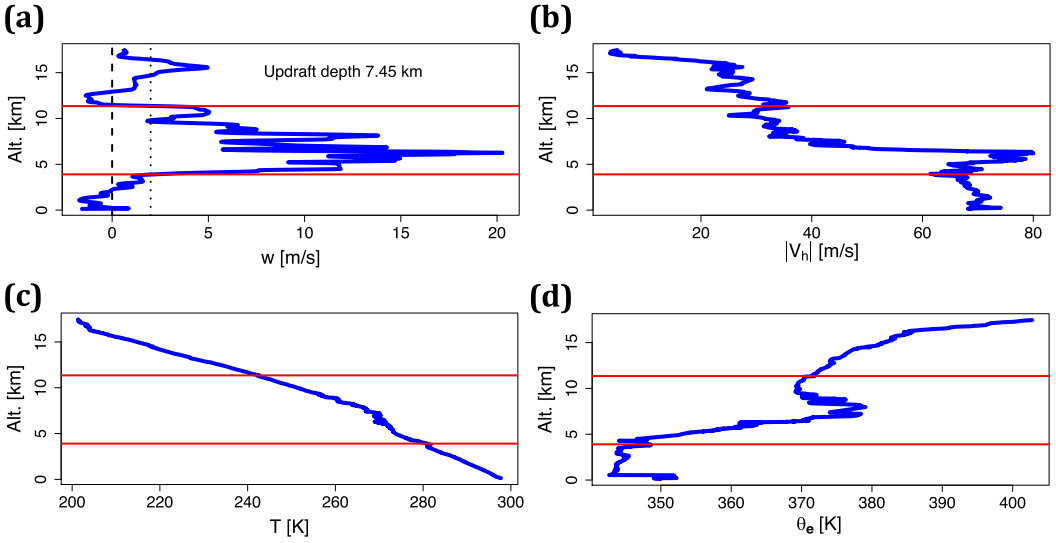

FIG. 7. Vertical profiles of (a) w, (b) $|V_h|$, (c) T, and (d) θ_e from an updraft sounding (dropsonde 72CC) launched into the eyewall of Patricia on 23 Oct. The red horizontal lines denote the depth of the updraft. The black long-dashed vertical line in (a) denotes $w = 0\,\mathrm{m\,s^{-1}}$. The black short-dashed vertical line in (a) denotes $w = 2\,\mathrm{m\,s^{-1}}$, which is the minimum, continuous, w strength required for an updraft. At least one data point within this region exceeds $4\,\mathrm{m\,s^{-1}}$, which classifies this sounding as an updraft sounding.

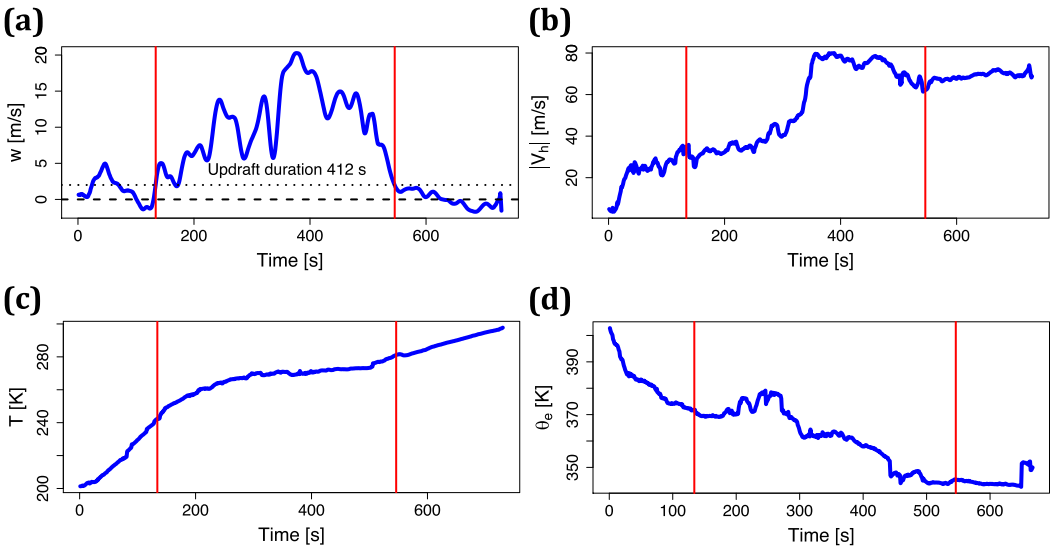

FIG. 8. As in Fig. 7, but with respect to time. The red vertical lines denote the time of the updraft. The black long-dashed horizontal line in (a) denotes $w = 0\ \mathrm{m\ s^{-1}}$. The black short-dashed horizontal line in (a) denotes $w = 2\ \mathrm{m\ s^{-1}}$, which is the minimum w strength required for an updraft.

w and θ_e to the mean updraft depth agree well with parcel buoyancy arguments and correlations between draft core diameters and mean w strength, and thermal buoyancy, in Eastin et al. (2005). In contrast to the updraft soundings, the downdraft soundings had near-zero or weakly negative correlations between the maximum downdraft depth and temporal autocorrelation scale, with no statistically significant relationships (Fig. 12). The positive correlations for updraft soundings indicate that there are, potentially, statistically significant relationships between the temporal autocorrelation scales and the depth of the updrafts, even though the mean and median temporal autocorrelation scales do not differ appreciably from the total dataset.

4. Discussion

From the large dataset of 437 XDDs in three TCs, it is evident that mean temporal autocorrelations were approximately 20–30 s for w, T, $|V_h|$, and θ_e, corresponding to an approximate altitudinal depth of 0.3–1.5 km, given

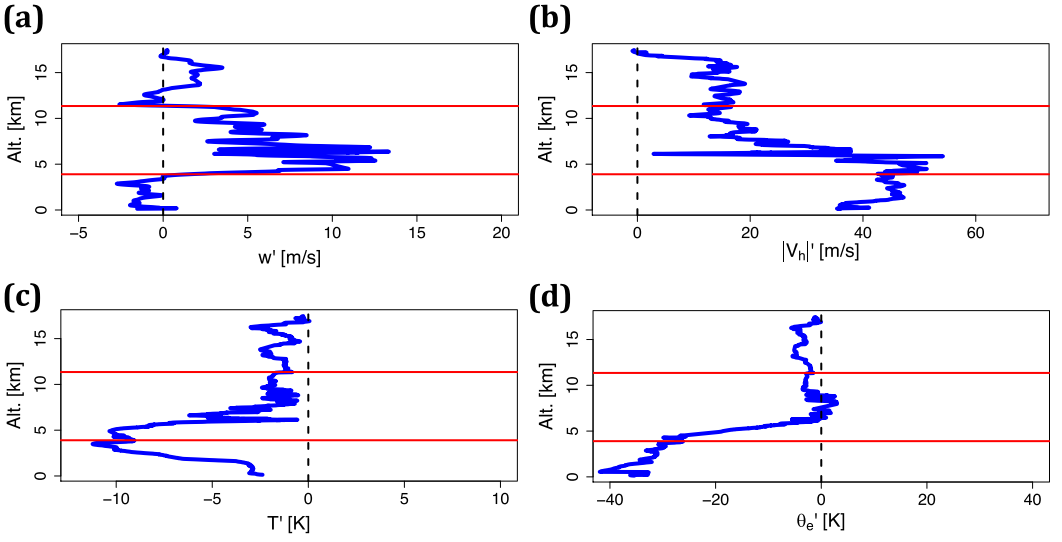

FIG. 9. As in Fig. 7, but for profiles of perturbation (a) w, (b) $|V_h|$, (c) T, and (d) θ_e. The black dashed vertical line denotes zero perturbation.

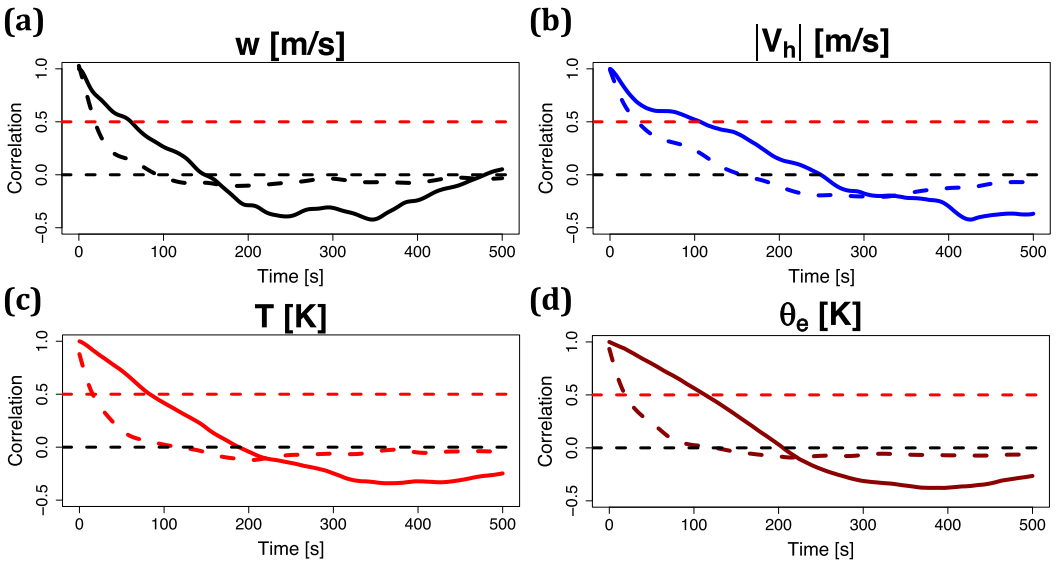

FIG. 10. Temporal autocorrelation correlograms of (a) w (black), (b) $|V_h|$ (blue), (c) T (red), and (d) θ_e (dark red). Correlations of 0.5 and 0.0 are denoted with horizontal dashed red and black lines, respectively. Correlograms for the single updraft sounding in Figs. 7–9 are solid curves, and correlograms for all soundings on 23 Oct are dashed curves.

the typical XDD fall speeds discussed in Nelson et al. (2019). The temporal autocorrelation scales suggest that interpolating sounding data to matching altitudes is, likely, justifiable within small 0.5-km intervals. The binning scheme used here and in Nelson et al. (2019) is finer than this estimate. These results also imply that the XDD sampling frequency adeptly oversampled the TCs in TCI.

From dropsonde to dropsonde, one of the conclusions that can be drawn is an estimate of the minimum spatial distribution of dropsondes needed to accurately depict a TC with transects of dropsondes from the observed atmospheric variables. Another way to phrase the previous statement is, "How close together can the XDDs be in TCs before adjacent data points become appreciably correlated?" The estimated spatial autocorrelation scales for all variables, except for w (Black et al. 1996; Lothon et al. 2006), are smaller than what was observed in previous studies (Table 1). Specifically, the $|V_h|$ and T estimated spatial autocorrelation scales are smaller for all observation days in the dataset (Wylie et al. 1985; Gunst 1995; Nichol and Wong 2008). This result is robust given that the median sounding spacing was also smaller than the autocorrelation scales shown by Wylie et al. (1985), Gunst (1995), and Nichol and Wong (2008).

The relatively high resolution of the original dataset could be why some of the autocorrelation length scales for the TCI data are smaller relative to past studies (Table 1). It is also plausible that the features measured by the non-TC studies were synoptic-scale features rather than mesoscale features, like in the three TCs observed during TCI, which would lead to smaller autocorrelation length scales or estimated spatial autocorrelation scales (Table 1). Regardless, the agreement between the spatial autocorrelations for w in this study and the spatial autocorrelations for w from radar data adjacent to updrafts and downdrafts in Black et al. (1996) is encouraging, and provides support for the findings herein.

It is important to note that one cannot truly know the spatial correlation limit without testing observations (like the XDDs) at a much higher launch rate/finer horizontal resolution. The autocorrelation spatial scales

TABLE 7. As in Table 5, but for soundings containing an updraft. Also included are the p values for the Student's t test comparisons between the temporal scales in Table 5 and the temporal scales in updraft soundings for each variable.

Day	Name	w	$\|V_h\|$	T	θ_e	RMW	Intensity
27 Sep	Marty	24	28	34	29	37	26
28 Sep	Marty	30	42	27	34	21	36
2 Oct	Joaquin	30	39	29	17	31	57
3 Oct	Joaquin	26	43	51	40	27	67
4 Oct	Joaquin	34	38	50	63	38	44
5 Oct	Joaquin	10	24	25	27	49	39
20 Oct	Patricia	5	19	14	17	77	15
21 Oct	Patricia	33	25	27	25	40	26
22 Oct	Patricia	19	28	15	14	19	59
23 Oct	Patricia	26	37	22	27	11	93
Mean	—	23.7	32.3	29.4	29.3	35	46
Median	—	26	32.5	27.0	27.0	34	41
Std dev	—	9.7	8.5	12.7	14.3	18	22
p	—	0.34	0.69	0.10	0.57		

TABLE 8. As in Table 7, but for soundings containing a downdraft.

Day	Name	w	$\lvert V_h\rvert$	T	θ_e	RMW	Intensity
27 Sep	Marty	8	21	10	32	37	26
28 Sep	Marty	27	23	23	29	21	36
2 Oct	Joaquin	26	41	28	21	31	57
3 Oct	Joaquin	32	47	67	38	27	67
4 Oct	Joaquin	0	0	0	0	38	44
5 Oct	Joaquin	0	0	0	0	49	39
20 Oct	Patricia	27	19	18	5	77	15
21 Oct	Patricia	21	31	21	24	40	26
22 Oct	Patricia	22	34	40	31	19	59
23 Oct	Patricia	20	71	17	20	11	93
Mean	—	22.9	35.9	28.0	25.0	35	46
Median	—	24.0	32.5	22.0	26.5	34	41
Std dev	—	6.7	16.1	16.9	10.1	18	22
p	—	0.40	0.47	0.35	0.71		

below the median, and even the minimum, horizontal sounding spacing (e.g., Patricia on 23 October; Tables 2 and 4) are estimates that are limited by the spacing of the original dataset. It can be confidently stated, however, that the true 0.5 autocorrelation spatial scales from day to day and storm to storm were smaller than the median sounding spacing, which was an average of 27 km on an individual date or 13 km for an individual TC. The relative agreement between the mean and median estimated spatial autocorrelation scales in Table 4 and Fig. 5 increases the confidence that these values are plausible and valid.

The medians for all of the individual days illustrate that w and θ_e had small estimated spatial autocorrelation scales between 4 and 6 km (Table 4). This agrees well with the model grid spacing required to resolve TC eyewall kinematics and physics (Gentry and Lackmann 2010). The estimated spatial autocorrelation scales for w and θ_e also agree well with the mean diameter of strong, buoyant updrafts documented in flight-level observations (e.g., Black et al. 1996; Eastin et al. 2005), which indicate that the spatial scales for these variables are governed at the convective scale and not the storm scale. The $\lvert V_h\rvert$ and T had slightly larger estimated spatial autocorrelation scales, with means/medians of approximately 7–11 km, which agrees well with the model grid spacing required to resolve features on the scale of the average RMW (approximately 55 km; Kimball and Mulekar 2004; Gentry and Lackmann 2010). When data were combined for each TC, w or θ_e always had the smallest estimated spatial autocorrelation scale, with the mean and median below 3 km; $\lvert V_h\rvert$ or T always had the largest estimated spatial autocorrelation scales for each TC between 3 and 6 km. The results, not surprisingly, imply that the spatial resolution of dropsondes needed to adequately depict the thermal or horizontal wind fields in transects of TCs is larger than what is needed to adequately depict convection and convection-related variables by approximately a factor of 2, assuming that the spatial autocorrelation scale estimates are accurate.

The spatial requirements of the XDDs for each atmospheric variable present an operational challenge for future TC dropsonde campaigns. The results of this study suggest that soundings should be, at a maximum, 10–20 km apart to accurately, and adequately, depict TC

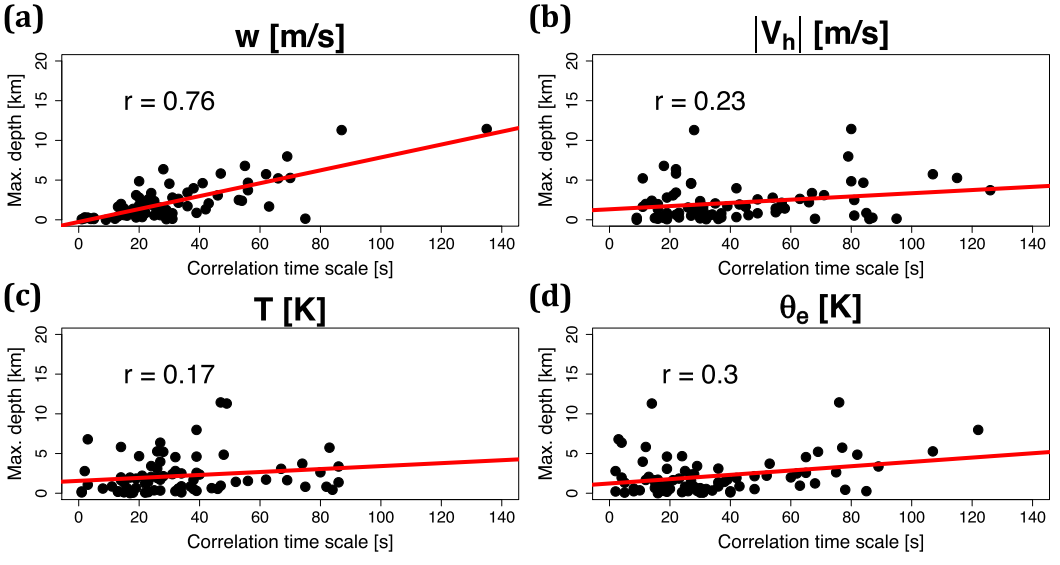

FIG. 11. The 0.5 autocorrelation temporal thresholds for (a) w, (b) $\lvert V_h\rvert$, (c) T, and (d) θ_e within individual soundings that recorded an updraft as a function of maximum updraft depth in the sounding. Correlations and linear fits (red lines) are also provided.

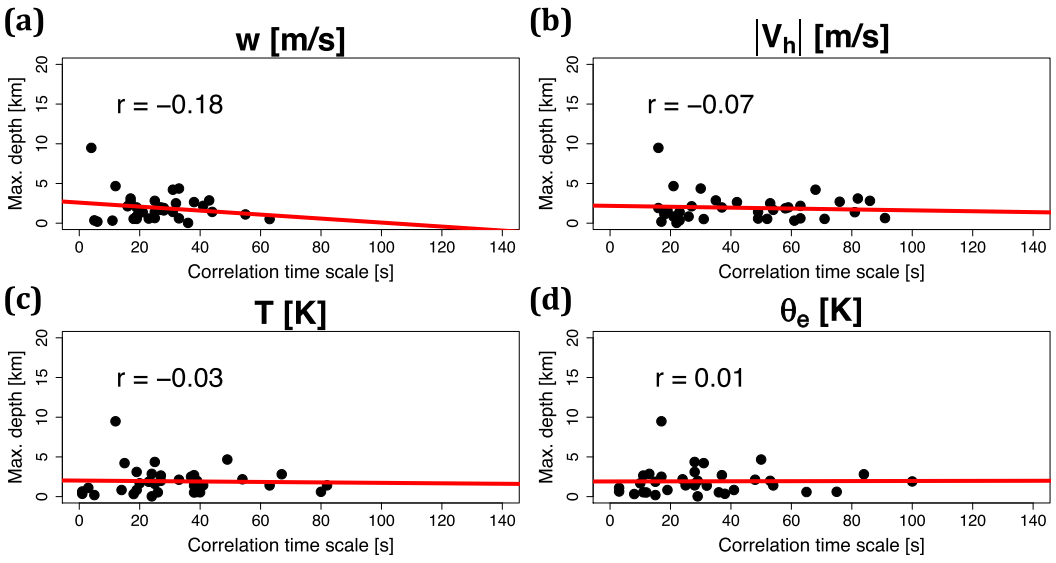

FIG. 12. As in Fig. 11, but for individual downdraft soundings and maximum downdraft depth in the sounding.

structure in transects of dropsondes. Further, the estimated spatial autocorrelation scales presented in this study suggest that the finest spatial resolution (approximately 3–4 km) and quickest launch frequency utilized in TCI was at the minimum limit of the required horizontal sampling interval needed to accurately, and adequately, depict TC structure in transects of dropsondes. In situations where the horizontal sampling interval was larger than 3–4 km, spatial interpolation cannot be accurately conducted and does not adequately depict the thermal or kinematic structure in the transects of these three TCs. The same conclusion can be made if dropsondes are launched at a resolution of 3–4 km, but one dropsonde fails. The latter situation suggests that a finer minimum and median horizontal spatial resolution of soundings than what was achieved during TCI should be used in future dropsonde-based TC campaigns.

If it is assumed that the estimated spatial autocorrelation scales in this study indicate the approximate scales of the observable features in the three TCs, then the spacing of observations required to accurately resolve those features can be estimated from the "$4\Delta x$ rule" (Grasso 2000). The results imply that the launch rate needs to be increased by approximately a factor of 4 to adequately resolve convection and thermal perturbations in transects of TCs, except for possible small-scale (smaller than 3 km) eyewall vortices (Grasso 2000; Gentry and Lackmann 2010). This assumes that the XDDs can adequately measure both weak and strong convection, since the expected vertical velocity errors are ± 1–$2\,\mathrm{m\,s^{-1}}$ (Nelson et al. 2019).

Understanding the temporal and spatial autocorrelations of dropsondes launched into TCs also plays an important role in modeling, and forecasting, TC track and intensity. The results of this study do not answer where and when to observe a TC, but the dropsonde spatial and temporal autocorrelations are important to modeling, and forecasting, studies examining the inclusion of targeted dropsonde observations, or dropsonde deniability (e.g., Langland 2005; Mu et al. 2009; Torn and Hakim 2009; Wu et al. 2009; Irvine et al. 2011; Romine et al. 2016). In targeted dropsonde studies, understanding autocorrelations with the XDDs allows scientists to know how many dropsondes would be needed to accurately resolve a targeted area without including highly correlated spatial data (e.g., Liu and Rabier 2003). For dropsonde deniability studies, removing a few dropsondes among a group of highly correlated dropsondes may not yield significant results. The w, $|V_h|$, T and θ_e horizontal autocorrelation scales found in the three TCs observed during TCI are considerably smaller than the typical length scales of background errors in models (Andersson et al. 1993; Irvine et al. 2011; Rizvi et al. 2012; Wang et al. 2014), and the horizontal autocorrelation scales are considerably smaller than the mean or median sampling intervals during TCI (Table 2). The results of this study, therefore, imply that this problem is unlikely to exist given the finest, mean, and median sampling intervals during TCI and the current sampling intervals of other research aircraft.

The results of this study also illustrate the complexity and operational challenges involved in depicting the thermodynamic and kinematic characteristics of the TC inner core. As a hypothetical situation, if a model with 2-km grid spacing and a domain size of 1000 km (order of magnitude of the diameter of the TCs observed

in TCI) were used and 50 XDDs were assimilated at one time (approximate number of XDDs launched each day during TCI), then the spacing of the XDDs would need to be 20 km apart (Liu and Rabier 2002; Gentry and Lackmann 2010). This assumes an equal spacing of dropsondes and an even distribution of dropsondes inside of the core and outside of the core. The hypothetical distance of 20 km is generally comparable to the median sounding spacings in the dataset, but larger than the daily estimated spatial autocorrelation scales for all variables examined by at least a factor of 2; however, the strong gradient regions of the core likely require a finer spatial resolution than outside of the core to accurately depict the thermodynamic and kinematic characteristics of the core.

Acknowledgments. The authors thank the Office of Naval Research (ONR) for support in this research and Patrick Duran and Chip N. Helms for insightful discussions. The ONR funded this research through the High Density Drop-Sonde Measurements Grant N000141712714. We also thank all of the principal investigators and others associated with TCI, including Yankee Environmental Systems.

REFERENCES

Aberson, S. D., 2008: Large forecast degradations due to synoptic surveillance during the 2004 and 2005 hurricane seasons. *Mon. Wea. Rev.*, **136**, 3138–3150, https://doi.org/10.1175/2007MWR2192.1.

Andersson, E., J. Pailleux, J. R. Eyre, A. P. McNally, G. A. Kelly, P. Courtier, and F. Rabier, 1993: Assimilation of satellite data by 3D-Var at ECMWF. *Seminar on Developments in the Use of Satellite Data in Numerical Weather Prediction*, Reading, United Kingdom, ECMWF, 167–188, https://www.ecmwf.int/node/7742.

Bell, M. M., and Coauthors, 2016: ONR tropical cyclone intensity 2015 NASA WB-57 HDSS dropsonde data, version 1.0. UCAR/NCAR Earth Observing Laboratory, accessed 1 March 2018, https://doi.org/10.5065/D6CF9NGC.

Biau, G., E. Zorita, H. von Storch, and H. Wackernagel, 1999: Estimation of precipitation by kriging in the EOF space of the sea level pressure field. *J. Climate*, **12**, 1070–1085, https://doi.org/10.1175/1520-0442(1999)012<1070:EOPBKI>2.0.CO;2.

Black, M. L., R. W. Burpee, and F. Marks Jr., 1996: Vertical motion characteristics of tropical cyclones determined with airborne Doppler radial velocities. *J. Atmos. Sci.*, **53**, 1887–1909, https://doi.org/10.1175/1520-0469(1996)053<1887:VMCOTC>2.0.CO;2.

Black, P., L. Harrison, M. Beaubien, R. Bluth, R. Woods, A. Penny, R. Smith, and J. Doyle, 2017: High Definition Sounding System (HDSS) for atmospheric profiling. *J. Atmos. Oceanic Technol.*, **34**, 777–796, https://doi.org/10.1175/JTECH-D-14-00210.1.

Black, R. A., H. B. Bluestein, and M. L. Black, 1994: Unusually strong vertical motions in a Caribbean hurricane. *Mon. Wea. Rev.*, **122**, 2722–2739, https://doi.org/10.1175/1520-0493(1994)122<2722:USVMIA>2.0.CO;2.

Brett, A. C., and S. E. Tuller, 1991: The autocorrelation of hourly wind speed observations. *J. Appl. Meteor.*, **30**, 823–833, https://doi.org/10.1175/1520-0450(1991)030<0823:TAOHWS>2.0.CO;2.

Bringi, V. N., L. Tolstoy, M. Thurai, and W. A. Petersen, 2015: Estimation of spatial correlation of drop size distribution parameters and rain rate using NASA's S-band polarimetric radar and 2D video disdrometer network: Two case studies from MC3E. *J. Hydrometeor.*, **16**, 1207–1221, https://doi.org/10.1175/JHM-D-14-0204.1.

Brooks, C. E. P., and N. B. Carruthers, 1978: *Handbook of Statistical Methods in Meteorology*. Amer. Meteor. Soc., 412 pp.

Doyle, J. D., and Coauthors, 2017: A view of tropical cyclones from above: The Tropical Cyclone Intensity (TCI) experiment. *Bull. Amer. Meteor. Soc.*, **98**, 2113–2134, https://doi.org/10.1175/BAMS-D-16-0055.1.

Eastin, M. D., P. G. Black, and W. M. Gray, 2002a: Flight-level thermodynamic instrument wetting errors in hurricanes. Part I: Observations. *Mon. Wea. Rev.*, **130**, 825–841, https://doi.org/10.1175/1520-0493(2002)130<0825:FLTIWE>2.0.CO;2.

——, ——, and ——, 2002b: Flight-level thermodynamic instrument wetting errors in hurricanes. Part II: Implications. *Mon. Wea. Rev.*, **130**, 842–851, https://doi.org/10.1175/1520-0493(2002)130<0842:FLTIWE>2.0.CO;2.

——, W. M. Gray, and P. G. Black, 2005: Buoyancy of convective vertical motions in the inner core of intense hurricanes. Part I: General statistics. *Mon. Wea. Rev.*, **133**, 188–208, https://doi.org/10.1175/MWR-2848.1.

Fisher, L., G. C. Craig, and C. Kiemle, 2013: Horizontal structure function and vertical correlation analysis of mesoscale water vapor variability observed by airborne lidar. *J. Geophys. Res. Atmos.*, **118**, 7579–7590, https://doi.org/10.1002/JGRD.50588.

Gentry, M. S., and G. M. Lackmann, 2010: Sensitivity of simulated tropical cyclone structure and intensity to horizontal resolution. *Mon. Wea. Rev.*, **138**, 688–704, https://doi.org/10.1175/2009MWR2976.1.

Gorman, R. M., 2009: Intercomparison of methods for the temporal interpolation of synoptic wind fields. *J. Atmos. Oceanic Technol.*, **26**, 828–837, https://doi.org/10.1175/2008JTECHO588.1.

Grasso, L. D., 2000: The difference between grid spacing and resolution and their application to numerical modeling. *Bull. Amer. Meteor. Soc.*, **81**, 579–580, https://doi.org/10.1175/1520-0477(2000)081<0579:CAA>2.3.CO;2.

Griffith, D. A., 2003: *Spatial Autocorrelation and Spatial Filtering: Gaining Understanding through Theory and Scientific Visualization*. Springer, 247 pp.

Gunst, R. F., 1995: Estimating spatial correlations from spatial–temporal meteorological data. *J. Climate*, **8**, 2454–2470, https://doi.org/10.1175/1520-0442(1995)008<2454:ESCFST>2.0.CO;2.

Habib, E., W. F. Krajewski, and G. J. Ciach, 2001: Estimation of rainfall interstation correlation. *J. Hydrometeor.*, **2**, 621–629, https://doi.org/10.1175/1525-7541(2001)002<0621:EORIC>2.0.CO;2.

Irvine, E. A., S. L. Gray, J. Methven, and I. A. Renfrew, 2011: Forecast impact of targeted observations: Sensitivity to observation error and proximity to steep orography. *Mon. Wea. Rev.*, **139**, 69–78, https://doi.org/10.1175/2010MWR3459.1.

Jameson, A. R., 2017: Spatial and temporal network sampling effects on the correlation and variance structures of rain observations. *J. Hydrometeor.*, **18**, 187–196, https://doi.org/10.1175/JHM-D-16-0129.1.

Janert, P. K., 2011: *Data Analysis with Open Source Tools*. O'Reilly, 509 pp.

Jorgensen, D. P., E. J. Zipser, and M. A. LeMone, 1985: Vertical motions in intense hurricanes. *J. Atmos. Sci.*, **42**, 839–856, https://doi.org/10.1175/1520-0469(1985)042<0839:VMIIH>2.0.CO;2.

Khalili, M., R. Leconte, and F. Brissette, 2007: Stochastic multisite generation of daily precipitation data using spatial autocorrelation. *J. Hydrometeor.*, **8**, 396–412, https://doi.org/10.1175/JHM588.1.

Kimball, S. K., and M. S. Mulekar, 2004: A 15-year climatology of North Atlantic tropical cyclones. Part I: Size parameters. *J. Climate*, **17**, 3555–3575, https://doi.org/10.1175/1520-0442(2004)017<3555:AYCONA>2.0.CO;2.

Langland, R. H., 2005: Issues in targeted observing. *Quart. J. Roy. Meteor. Soc.*, **131**, 3409–3425, https://doi.org/10.1256/qj.05.130.

LeMone, M. A., and E. J. Zipser, 1980: Cumulonimbus vertical velocity events in GATE. Part I: Diameter, intensity, and mass flux. *J. Atmos. Sci.*, **37**, 2444–2457, https://doi.org/10.1175/1520-0469(1980)037<2444:CVVEIG>2.0.CO;2.

Leutbecher, M., J. Barkmeijer, T. N. Palmer, and A. J. Thorpe, 2002: Potential improvement of forecasts of two severe storms using targeted observations. *Quart. J. Roy. Meteor. Soc.*, **128**, 1641–1670, https://doi.org/10.1002/qj.200212858313.

Liu, Z. Q., and F. Rabier, 2002: The interaction between model resolution, observation resolution and observation density in data assimilation: A one-dimensional study. *Quart. J. Roy. Meteor. Soc.*, **128**, 1367–1386, https://doi.org/10.1256/003590002320373337.

——, and ——, 2003: The potential of high-density observations for numerical weather prediction: A study with simulated observations. *Quart. J. Roy. Meteor. Soc.*, **129**, 3013–3035, https://doi.org/10.1256/qj.02.170.

Lothon, M., D. H. Lenschow, and S. D. Mayor, 2006: Coherence and scale of vertical velocity in the convective boundary layer from a Doppler lidar. *Bound.-Layer Meteor.*, **121**, 521–536, https://doi.org/10.1007/s10546-006-9077-1.

Molinari, J., D. Vollaro, and S. Skubis, 1993: Application of the Eliassen balanced model to real-data tropical cyclones. *Mon. Wea. Rev.*, **121**, 2409–2419, https://doi.org/10.1175/1520-0493(1993)121<2409:AOTEBM>2.0.CO;2.

Mu, M., F. Zhou, and H. Wang, 2009: A method for identifying the sensitive areas in targeted observations for tropical cyclone prediction: Conditional nonlinear optimal perturbation. *Mon. Wea. Rev.*, **137**, 1623–1639, https://doi.org/10.1175/2008MWR2640.1.

Nelson, T. C., L. C. Harrison, and K. L. Corbosiero, 2019: Examination of the Expendable Digital Dropsonde–derived vertical velocities from the Tropical Cyclone Intensity (TCI) experiment. *Mon. Wea. Rev.*, **147**, 2367–2386, https://doi.org/10.1175/MWR-D-18-0414.1.

Nichol, J. E., and M. S. Wong, 2008: Spatial variability of air temperature and appropriate resolution for satellite-derived air temperature estimation. *Int. J. Remote Sens.*, **29**, 7213–7223, https://doi.org/10.1080/01431160802192178.

Pérez, I. A., M. Á. García, M. L. Sánchez, and B. Torre, 2004: Autocorrelation analysis of meteorological data from a RASS sodar. *J. Appl. Meteor.*, **43**, 1213–1223, https://doi.org/10.1175/1520-0450(2004)043<1213:AAOMDF>2.0.CO;2.

Privé, N. C., and R. M. Errico, 2016: Temporal and spatial interpolation errors of high-resolution modeled atmospheric fields. *J. Atmos. Oceanic Technol.*, **33**, 303–311, https://doi.org/10.1175/JTECH-D-15-0132.1.

Raymond, D. J., G. B. Raga, C. S. Bretherton, J. Molinari, C. López-Carrillo, and Ž. Fuchs, 2003: Convective forcing in the intertropical convergence zone of the eastern Pacific. *J. Atmos. Sci.*, **60**, 2064–2082, https://doi.org/10.1175/1520-0469(2003)060<2064:CFITIC>2.0.CO;2.

Rizvi, S. R. H., Z. Liu, and X.-Y. Huang, 2012: Generation of WRF-ARW background errors (BE) for GSI. NCAR Rep., 29 pp., https://dtcenter.org/com-GSI/users/docs/write_ups/WRF-ARW-GSI_BE.pdf.

Rogers, R. F., and Coauthors, 2017: Rewriting the tropical record books: The extraordinary intensification of Hurricane Patricia. *Bull. Amer. Meteor. Soc.*, **98**, 2091–2112, https://doi.org/10.1175/BAMS-D-16-0039.1.

Romine, G. S., C. S. Schwartz, R. D. Torn, and M. L. Weisman, 2016: Impact of assimilating dropsonde observations from MPEX on ensemble forecasts of severe weather events. *Mon. Wea. Rev.*, **144**, 3799–3823, https://doi.org/10.1175/MWR-D-15-0407.1.

Stern, D. P., G. H. Bryan, and S. D. Aberson, 2016: Extreme low-level updrafts and wind speeds measured by dropsondes in tropical cyclones. *Mon. Wea. Rev.*, **144**, 2177–2204, https://doi.org/10.1175/MWR-D-15-0313.1.

Torn, R. D., and G. J. Hakim, 2009: Ensemble data assimilation applied to RAINEX observations of Hurricane Katrina (2005). *Mon. Wea. Rev.*, **137**, 2817–2829, https://doi.org/10.1175/2009MWR2656.1.

Venables, W. N., and B. D. Ripley, 2002: *Modern Applied Statistics with S*. 4th ed. Springer, 504 pp.

Wang, H., X. Y. Huang, J. Sun, D. Xu, M. Zhang, S. Fan, and J. Zhong, 2014: Inhomogeneous background error modeling for WRF-Var using the NMC method. *J. Appl. Meteor. Climatol.*, **53**, 2287–2309, https://doi.org/10.1175/JAMC-D-13-0281.1.

Willoughby, H. E., 1990: Gradient balance in tropical cyclones. *J. Atmos. Sci.*, **47**, 265–274, https://doi.org/10.1175/1520-0469(1990)047<0265:GBITC>2.0.CO;2.

Wu, C., and Coauthors, 2009: Intercomparison of targeted observation guidance for tropical cyclones in the northwestern Pacific. *Mon. Wea. Rev.*, **137**, 2471–2492, https://doi.org/10.1175/2009MWR2762.1.

Wylie, D. P., B. B. Hinton, M. R. Howland, and R. J. Lord, 1985: Autocorrelation of wind observations. *Mon. Wea. Rev.*, **113**, 849–857, https://doi.org/10.1175/1520-0493(1985)113<0849:AOWO>2.0.CO;2.